Hydrocarbon seepage in the deep seabed links subsurface and seafloor biospheres

Anirban Chakraborty[a,1], S. Emil Ruff[b,c], Xiyang Dong[a,d,e], Emily D. Ellefson[a,b], Carmen Li[a], James M. Brooks[f], Jayme McBee[f], Bernie B. Bernard[f], and Casey R. J. Hubert[a,1]

[a]Department of Biological Sciences, University of Calgary, Calgary, AB T2N 1N4, Canada; [b]Department of Geoscience, University of Calgary, Calgary, AB T2N 1N4, Canada; [c]Ecosystems Center and J. Bay Paul Center for Comparative Molecular Biology and Evolution, Marine Biological Laboratory, Woods Hole, MA 02543; [d]School of Marine Sciences, Sun Yat-Sen University, 519082 Zhuhai, People's Republic of China; [e]Southern Marine Science and Engineering Guangdong Laboratory (Zhuhai), 519000 Zhuhai, People's Republic of China; and [f]TDI-Brooks International, College Station, TX 77845

Edited by David M. Karl, University of Hawaii at Manoa, Honolulu, HI, and approved March 26, 2020 (received for review February 6, 2020)

Marine cold seeps transmit fluids between the subseafloor and seafloor biospheres through upward migration of hydrocarbons that originate in deep sediment layers. It remains unclear how geofluids influence the composition of the seabed microbiome and if they transport deep subsurface life up to the surface. Here we analyzed 172 marine surficial sediments from the deep-water Eastern Gulf of Mexico to assess whether hydrocarbon fluid migration is a mechanism for upward microbial dispersal. While 132 of these sediments contained migrated liquid hydrocarbons, evidence of continuous advective transport of thermogenic alkane gases was observed in 11 sediments. Gas seeps harbored distinct microbial communities featuring bacteria and archaea that are well-known inhabitants of deep biosphere sediments. Specifically, 25 distinct sequence variants within the uncultivated bacterial phyla *Atribacteria* and *Aminicenantes* and the archaeal order *Thermoprofundales* occurred in significantly greater relative sequence abundance along with well-known seep-colonizing members of the bacterial genus *Sulfurovum*, in the gas-positive sediments. Metabolic predictions guided by metagenome-assembled genomes suggested these organisms are anaerobic heterotrophs capable of nonrespiratory breakdown of organic matter, likely enabling them to inhabit energy-limited deep subseafloor ecosystems. These results point to petroleum geofluids as a vector for the advection-assisted upward dispersal of deep biosphere microbes from subsurface to surface environments, shaping the microbiome of cold seep sediments and providing a general mechanism for the maintenance of microbial diversity in the deep sea.

deep biosphere | microbiome | dispersal

Deep-sea sediments found in greater than 1,000-m water depth cover half of the Earth's surface. Unlike at shallow continental margins, abyssal sedimentary ecosystems are generally oligotrophic due to negligible local primary productivity, extremely slow rates of sediment deposition, and limited influx of organic matter (1). Despite these conditions, sediments in and beneath the deep ocean floor harbor a diverse microbiome, with microbial life detected in the deepest points in the ocean (2) as well as down to kilometers below the seafloor (3, 4). Such subseafloor habitats experience varying thermochemical gradients across geological horizons (5) and remain connected to the overlying oceans through unique geological features such as marine cold seeps (6, 7), submarine mud volcanoes (8), and midocean ridge-associated vents or seamounts (9). Organic-rich geofluids from the warm subsurface emanate up and out of the cold seafloor at these sites.

Because of their ability to constantly deliver organic substrates and inorganic energy sources, marine cold seeps, mud volcanoes, and hydrothermal vents create geochemical and biological oases in the seabed (7, 9). Cold seeps are particularly diverse in terms of the chemical composition of the seeping hydrocarbons, with some expelling a mixture of thermogenic liquid and gaseous hydrocarbons sourced from deep petroleum reservoirs and others emitting biogenic methane produced in shallower sediment layers (10). Emigrating geofluids support locally selected and largely distinct microbial communities relative to the surrounding seabed microbiome, resulting in biodiversity hotspots (11, 12). Recent investigations focusing on the distribution of thermophilic endospores in hydrocarbon-associated sediments (13) and on microbial dispersal via mud volcanoes (14, 15) suggest that upward migration of subsurface microbes into the seabed occurs via ebullition. Hydrocarbons and other gases in mud volcanic discharges allow for an overpressurized buoyancy-driven transport of sediment being expelled to the surface through an overlying crater (8). Cold seeps, which are much more widespread in the global ocean than mud volcanoes (16), experience similar buoyancy-driven geofluid flow through saturated porous sediments but do not physically transport the same large volumes of subsurface material that mud volcanoes do (17). It is therefore less clear whether cold seeps can similarly achieve the upward transportation of microbial cells, and to which extent gas-rich fluids are a dominant vector for deep-to-shallow microbe dispersal in the marine environment.

The Gulf of Mexico (GoM) basin is well known for widespread natural seepage of petroleum-derived thermogenic hydrocarbons

Significance

The marine subsurface is one of the largest habitats on Earth composed exclusively of microorganisms and harboring on the order of 10^{29} microbial cells. It is unclear if deep subsurface life impacts overlying seafloor diversity and biogeochemical cycling in the deep ocean. We analyzed the microbial communities of 172 seafloor surface sediment samples, including gas and oil seeps as well as sediments not subject to upward fluid flow. A strong correlation between typical subsurface clades and active geofluid seepage suggests that subsurface life is injected into the deep ocean floor at hydrocarbon seeps, a globally widespread hydrogeological phenomenon. This supply of subsurface-derived microbial populations, biomass, and metabolic potential thus increases biodiversity and impacts carbon cycling in the deep ocean.

Author contributions: A.C. and C.R.J.H. designed research; A.C., S.E.R., X.D., E.D.E., C.L., J.M.B., and B.B.B. performed research; A.C., S.E.R., X.D., J.M.B., J.M., and B.B.B. analyzed data; and A.C., S.E.R., X.D., and C.R.J.H. wrote the paper.

The authors declare no competing interest.

This article is a PNAS Direct Submission.

Data deposition: DNA sequences (amplicon and metagenome raw sequences) have been deposited in NCBI's Sequence Read Archive (SRA) under BioProject accession numbers PRJNA511010 and PRJNA485648.

[1]To whom correspondence may be addressed. Email: anirban.chakraborty@ucalgary.ca or chubert@ucalgary.ca.

This article contains supporting information online at https://www.pnas.org/lookup/suppl/doi:10.1073/pnas.2002289117/-/DCSupplemental.

First published April 30, 2020.

sourced from deeply buried oil and gas reservoirs. The composition and activity of cold-adapted microbial communities at GoM seeps have been studied in detail in relation to the impact of hydrocarbons on biodiversity (18) and hydrocarbon biodegradation (19). Efforts to distinguish between different seep habitats in the GoM basin have largely focused on geochemical assessments of migrating fluids and gases, with an emphasis on readily accessible northern locations found in shallow water (6). Cold seeps situated in the deep water Eastern GoM (EGoM) have received much less attention regarding hydrocarbon geochemistry and microbial diversity. Using sediments from 172 locations in the EGoM we investigated whether sediments experiencing advective migration of gas- or oil-rich fluids harbor distinct microbiomes, and whether subsurface-derived taxa can be identified and correlated to migrated gas or oil. Detailed gas and oil geochemistry were combined with rRNA gene-based biodiversity surveillance and shotgun metagenomic sequencing, enabling correlations between specific microbial taxa and multiple hydrocarbon parameters to be determined and interpreted based on metabolic predictions from metagenome-assembled genomes. This revealed evidence of deep-to-shallow microbial dispersal significantly associated with seepage of gaseous hydrocarbons in these deep-sea sediments.

Results

Migrated Hydrocarbons in EGoM Sediments. Piston cores from 172 locations covered a wide range of water depths (132 to 3,395 m) including 134 locations deeper than 2,000 m (Fig. 1 and *SI Appendix*, Table S1). Light hydrocarbon gases (C_1–C_5) and migrated oil (C_{6+} liquid hydrocarbons) were investigated at all locations and are presented as the mean of individual measurements obtained from three depth intervals within the sediment cores (Fig. 2). The major parameters used to monitor the light hydrocarbon gases were the concentrations of total and C_{2+} alkane gases (Fig. 2*A*). Total alkane gases showed a wide distribution of 1 to 135,448 parts per million by volume (ppmv) across all locations. Only a small fraction of sediment cores (n = 11) contained >10,000 ppmv of light hydrocarbon gases and were considered "gas-positive" in this study. Distribution of C_{2+} alkane gases was strongly correlated with the total alkane gases (adjusted $R^2 = 0.651$, $F_{1,170} = 320.6$, $P < 2.2e^{-16}$) despite higher alkane gases representing relatively minor fractions (0.01 to 2.01%) of the total gases. Comparing the ratio of methane to

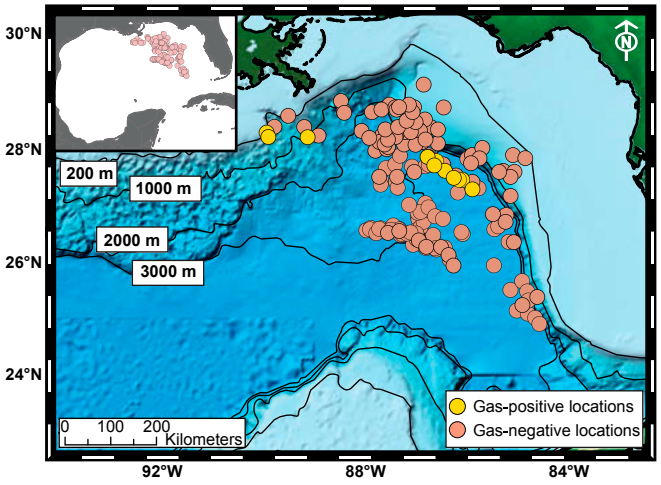

Fig. 1. Location and bathymetric profile of the EGoM sediment cores. Map of the Eastern Gulf of Mexico showing the 172 sampling locations and bathymetry of the study area. Symbol colors indicate the gas-positive and gas-negative locations. The *Inset* map shows the extent of the study area relative to the entire GoM basin. Maps were drawn using ArcGIS Desktop 10.4.

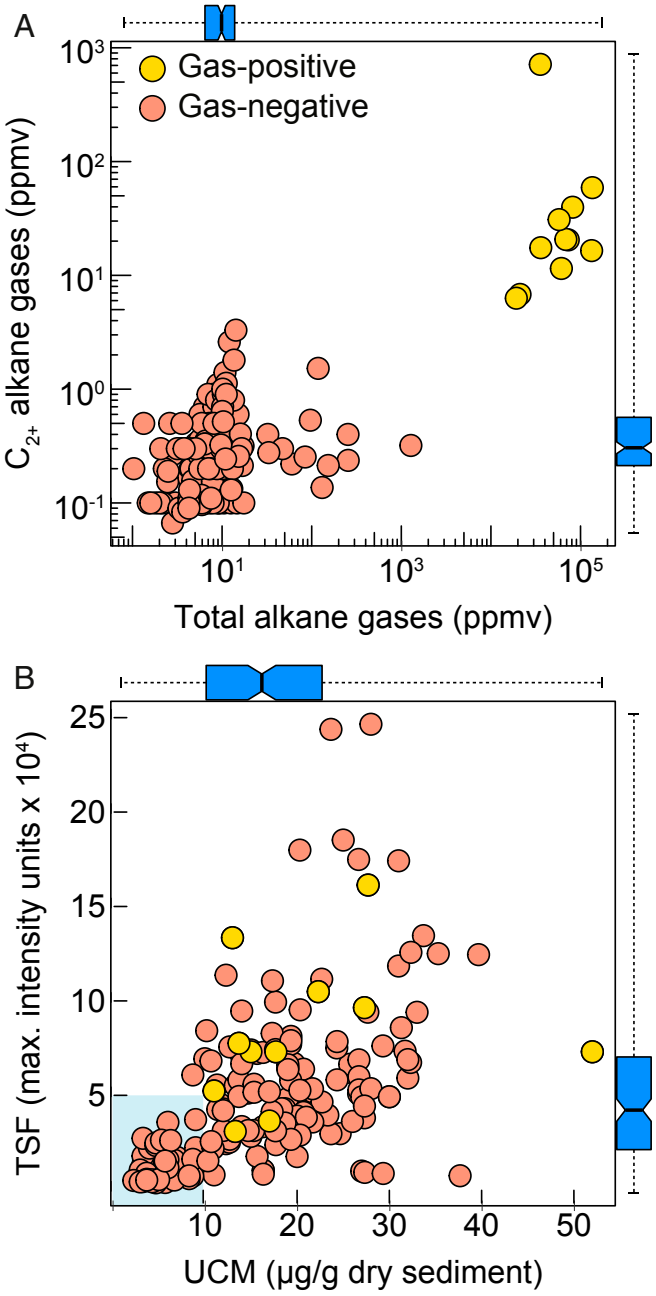

Fig. 2. Hydrocarbon characterization of the EGoM sediment cores. Scatterplots showing the mean values (n = 3 extracts per core) of the geochemical parameters used for assessing the gaseous (*A*) and liquid (*B*) hydrocarbon content in sediment cores. Symbol colors represent gaseous hydrocarbon categories as determined by total alkane gas concentrations greater than 10,000 ppmv. The major gas and oil parameters are also summarized by marginal box-and-whisker plots (minimum, lower quartile, median, upper quartile, and maximum) beside the corresponding axes. The light blue shaded area in *B* highlights thresholds of UCM (≥10 µg/g) and TSF maximum intensity (≥50,000) for assessing the presence of oil in the EGoM sediment cores.

combined ethane and propane concentrations [$C_1/(C_2+C_3)$] and the carbon isotopic compositions of methane ($\delta^{13}C_1$) in EGoM gas-positive samples (*SI Appendix*, Fig. S1*A*) further showed that the $C_1/(C_2+C_3)$ ratio for most of the EGoM samples remained in the >1,000 range while contributions of biogenic methane were evident from $\delta^{13}C_1$ values being more negative than −60‰ (20). Historic hydrocarbon data obtained from elsewhere in

the GoM reveal that these 11 gas-positive sediments are similar to many other gassy sites throughout this basin (*SI Appendix*, Fig. S1*B*).

The presence of liquid hydrocarbons in the cores was assessed by measuring the mass of the unresolved complex mixture (UCM) and the total scanning fluorescence (TSF) intensity in all 172 sediments. UCM and TSF are often used as major indicators of migrated oil (13, 21). The UCM represents a suite of biodegraded saturated hydrocarbons that are not easily separated using gas chromatography, resulting in a hump-shaped baseline with numerous smaller peaks representing individual compounds. TSF intensities on the other hand are generally independent of microbial alteration of hydrocarbon compounds and provide a measure of petroleum-related aromatic hydrocarbon concentrations. When compared against each other, the "thermogenicity trend" of these two parameters remains linear over several orders of magnitude (21). Mean UCM and TSF values generally ranged from 2 to 52 μg/g dry sediment and 1,800 to 244,668 intensity units, respectively. These two parameters were positively correlated (adjusted $R^2 = 0.281$, $F_{1,170} = 66.5$, $P < 7.4e^{-14}$) among all locations (Fig. 2*B*). Minimum thresholds for UCM (10 μg/g dry sediment) and TSF (50,000 intensity units) were used to eliminate hydrocarbon signatures not sourced from the subsurface (13). By these criteria, all 11 gas-positive sediments also qualified for unambiguous occurrence of migrated oil. The presence of oil within EGoM sediments was more widespread compared to the presence of gas, with a further 121 out of the 161 gas-negative locations being qualified for oil.

Microbial Diversity and Community Structure in EGoM Sediments. Genomic DNA extracted from near-surface sediments representing 0 to 20 centimeters below seafloor (cmbsf) was used to construct bacterial and archaeal 16S rRNA gene amplicon libraries. Analysis of variance (ANOVA) confirmed that observed and estimated (Chao1) richness of both bacterial and archaeal communities within gas-positive and gas-negative locations were significantly different ($p.adj < 0.05$; *SI Appendix*, Fig. S2). Relatedness between bacterial and archaeal diversity was further corroborated by a Mantel test (Mantel statistic $r = 0.85$; $P < 0.001$) using Bray–Curtis dissimilarity indices. The top 10 bacterial phyla representing 84.5% of the bacterial sequences were *Proteobacteria* (34.5%), *Chloroflexi* (20.4%), *Acidobacteria* (6.5%), *Nitrospirae* (4.2%), *Aminicenantes* (formerly OP8; 4.1%), *Actinobacteria* (4%), *Aerophobetes* (formerly CD12; 3.4%), *Firmicutes* (2.6%), *Atribacteria* (formerly JS1 and OP9; 2.6%), and *Nitrospinae* (2.2%) (*SI Appendix*, Fig. S3*A*). Prominent archaeal phyla that represented 95.7% of the archaeal sequences were *Thaumarchaeota* (51.1%), *Crenarchaeota* (14.3%), *Asgardaeota* (13.7%), *Nanoarchaeota* (13.2%), and *Euryarchaeota* (3.4%) (*SI Appendix*, Fig. S3*B*).

Permutational multivariate analysis of variance coupled with false discovery rate correction, and analysis of similarities conducted with bacterial and archaeal communities showed that the gas-positive locations harbored significantly dissimilar bacterial (PERMANOVA pseudo$F = 3.596$, $p.adj = 0.0009$, 999 permutations; ANOSIM $R = 0.36$, $P = 0.001$) and archaeal (PERMANOVA pseudo$F = 1.895$, $p.adj = 0.019$, 999 permutations; ANOSIM $R = 0.17$, $P = 0.034$) communities (Fig. 3 *A* and *B*). Repeating this analysis with locations grouped based on the presence of oil in the cores resulted in community dissimilarity not being significant, for either bacteria (PERMANOVA pseudo$F = 1.605$, $p.adj = 0.092$, 999 permutations; ANOSIM $R = 0.015$, $P = 0.634$) or archaea (PERMANOVA pseudo$F = 1.882$, $p.adj = 0.072$, 999 permutations; ANOSIM $R = 0.077$, $P = 0.479$) (Fig. 3 *C* and *D*). Partial distance-based redundancy analysis using total alkane gases, total C_{2+} alkane gases, UCM, and TSF as constraining variables further indicated that total alkane gases best explains bacterial and archaeal community dissimilarity between gas-positive and gas-negative locations (Fig. 3 *E* and *F*). Correlation analyses of the gaseous and liquid hydrocarbon parameters with community composition showed that both total and C_{2+} alkane gases had maximum correlation with bacterial and archaeal communities among all possible subsets (Spearman's rank correlations of 0.223 and 0.218, respectively), suggesting that advection of gas-rich fluids exerts a strong influence on community dissimilarity in gas-positive sediments.

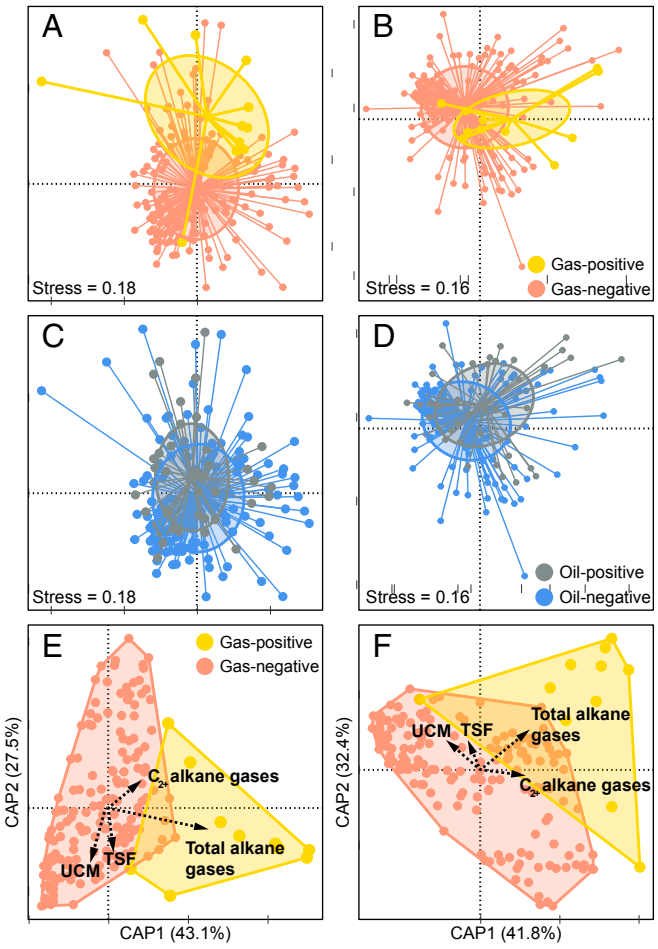

Fig. 3. Community similarity within the EGoM sediments. Similarity of microbial communities visualized by two-dimensional (2D) nonmetric multidimensional scaling (NMDS) when samples are grouped based on the presence of gas (*A* and *B*) or oil (*C* and *D*). Bacterial communities are visualized in *A* and *C* while archaeal communities are shown in *B* and *D*. A distance-based redundancy analysis (db-RDA) showing bacterial (*E*) and archaeal (*F*) community similarity when total alkane gases, total C_{2+} alkane gases, UCM, and TSF were used as constraining variables and were fitted onto the ordination as arrows. The length of each arrow indicates the multiple partial correlation of the variable to RDA axes and can be interpreted as an indication of that variable's contribution to the explained community similarity. Significance of RDA was tested by ANOVA for both bacterial ($F = 1.845$, $P < 0.001$) and archaeal ($F = 1.898$, $P < 0.001$) communities. In *A*–*D*, each sample (dot) is connected to the weighted averaged mean of the within-group distances and the ellipses represent one SD of the weighted averaged mean. The amplicon libraries were subsampled to 5,000 (bacteria) and 3,500 (archaea) reads in order to account for uneven sequencing depth and to ensure comparability of sample diversity.

Association of Subsurface Lineages with Gas Seepage. Members of the bacterial phyla *Atribacteria* and *Aminicenantes* were present in significantly greater abundance in the 11 gas-positive locations (Fig. 4 *A* and *B*), as were members of the genus *Sulfurovum*

within the phylum *Campylobacterota* (formerly class *Epsilonproteobacteria*) (22) and members of the archaeal order *Thermoprofundales* (formerly Marine Benthic Group D) (23). This was confirmed by differential abundance analysis at various taxonomic levels using a negative binomial distribution model implemented in the R package DESeq2 (24) (*SI Appendix*, Table S2). Closely related *Atribacteria*, *Aminicenantes*, and *Thermoprofundales* are frequently detected in deeper subsurface sediments (1, 25–28). Consistent with this, comparison of the relative sequence abundances of these taxa at three sediment depth regimes (0 to 20, 40 to 60, and 80 to 100 cmbsf) from one gas-positive and three gas-negative sediment cores revealed that these three lineages were more abundant in the deeper sediments, whereas *Sulfurovum* was detected only in the uppermost section (Fig. 4 *C* and *D*). *Atribacteria*, *Aminicenantes*, and *Thermoprofundales* had comparable abundances in the deeper sections of all four cores regardless of the presence of gas. Within the topmost section, however, these lineages were severely diminished in the three gas-negative cores (Fig. 4*D*) relative to the gas-positive core.

Atribacteria and *Sulfurovum* were represented by 65 and 12 amplicon sequence variants (ASVs), respectively, whereas the other two groups had greater diversity with 289 *Aminicenantes* ASVs and 160 *Thermoprofundales* ASVs, the majority occurring in low relative sequence abundance. In order to investigate the correlation of the relative sequence abundances of these ASVs with the hydrocarbon parameters, we first removed the ASVs occurring in fewer than 5 out of the 172 locations. Distributions of relative sequence abundances of each of the remaining 91 ASVs were used to conduct pairwise Pearson's correlation analysis with the distribution of each of the four gas and oil parameters. A total of 25 ASVs (*Atribacteria* = 13, *Aminicenantes* = 6, *Sulfurovum* = 2, and *Thermoprofundales* = 4) were found to be significantly correlated ($P < 0.05$) with both total and C_{2+} alkane gases (hereafter referred to as gas-associated ASVs; Fig. 4*E* and *SI Appendix*, Table S3). None of these ASVs showed similar correlation with the oil parameters UCM and TSF. Pairwise co-occurrence analysis of the 25 gas-associated ASVs further revealed that 12 out of the 21 bacteria co-occurred with the three most abundant archaea (Fig. 4*F*). Individually, the gas-associated ASVs represented <2% mean relative sequence abundance in the gas-positive sediment microbial communities (*SI Appendix*, Fig. S4).

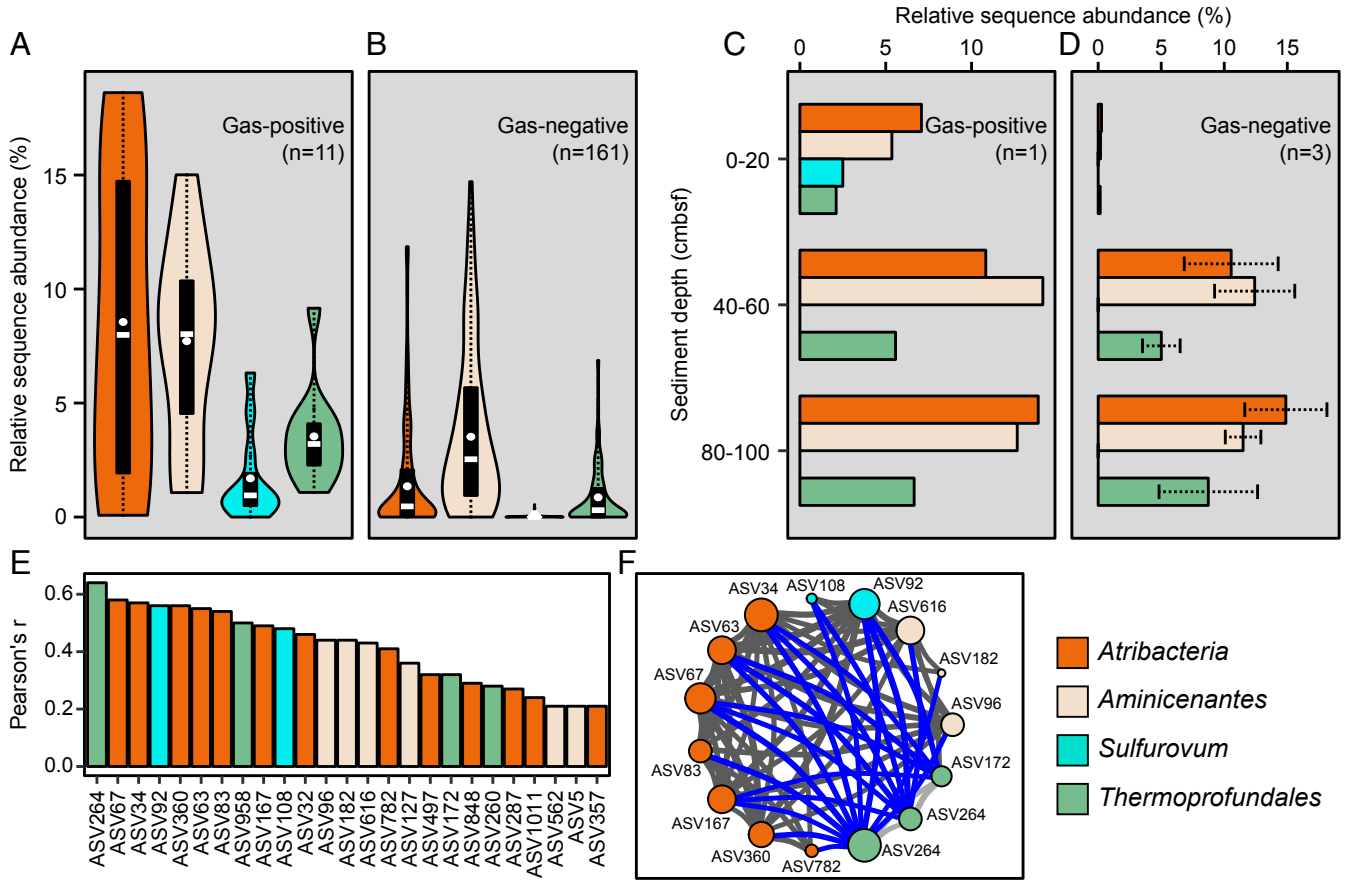

Fig. 4. Distribution and co-occurrence of gas-associated lineages. Relative sequence abundances of *Atribacteria*, *Aminicenantes*, *Sulfurovum*, and *Thermoprofundales* in near-surface sediments within the gas-positive and the gas-negative locations (*A* and *B*), visualized by kernel density distribution in violin plots. Embedded black box and whiskers indicate minimum, lower quartile, upper quartile, and maximum values. The thick white horizontal line and the white dot within each box represent the median and the mean of the distribution, respectively. Sequence abundances of the above four lineages in three sediment depths within a gas-positive (*C*) and three gas-negative (*D*) sediment cores, respectively, are shown using horizontal bar plots. Pearson's correlation coefficients of each of the 25 gas-associated ASVs from these four lineages with total alkane gases are shown in *E*. Co-occurrence of 15 gas-associated ASVs (*Atribacteria* = 7, *Aminicenantes* = 3, *Thermoprofundales* = 3, and *Sulfurovum* = 2) are shown in a network diagram (*F*) where each node represents an ASV and a line joining two nodes represents co-occurrence of two ASVs. The size of the nodes indicates its degree of connectivity and the thickness of the lines indicates strength of correlation. The blue, solid gray, and light gray colored lines indicate connections between bacterial and archaeal, within bacterial and within archaeal ASVs, respectively. Symbol colors represent taxonomic affiliations of the four lineages.

Phylogeny of Gas-Associated ASVs. Among these lineages, *Atribacteria* showed the most significantly elevated sequence abundance in the gas-positive locations (*SI Appendix*, Table S2). This phylum also contained the largest number of gas-associated ASVs (n = 13) including 5 of the top 7 ASVs showing the strongest correlation with the total alkane gases (Fig. 4*E*). To investigate the phylogeny of *Atribacteria* ASVs and their close relatives, a high-resolution phylogenetic tree was calculated based on >1,100 near-full-length 16S rRNA gene sequences from the SILVA nonredundant (NR) small subunit (SSU) ribosomal database (release 132, December 2017) (29) and the National Center for Biotechnology Information (NCBI) nucleotide database (as of June 2018). A consensus tree supported by four separate phylogenetic reconstructions (*Methods*) demonstrated that the phylum *Atribacteria* is comprised of two class-level clades, corresponding to the OP9 and JS1 divisions (*SI Appendix*, Fig. S5). Based on minimum sequence identity (MSI) thresholds for taxonomy using the 16S rRNA gene (30), OP9 comprises one order-level clade (MSI cutoff: 83.6%) and JS1 comprises two order-level clades. *Atribacteria* contains at least 11 family-level clades (MSI cutoff: 87.7%) and a larger and rapidly growing number of genus-level clades (MSI: 94.8%; not shown) as this phylum continues to be the focus of new discoveries (28, 31, 32). The 13 gas-associated *Atribacteria* ASVs are all affiliated with the same family within JS1 (*SI Appendix*, Fig. S5). Fig. 5 shows that most of these cluster among three genus-level clades consisting almost exclusively of sequences from deep subseafloor habitats as well as seep and near-seep habitats impacted by subseafloor geofluids. Similarly, gas-associated ASVs belonging to *Aminicenantes* (n = 6) and *Thermoprofundales* (n = 4) were also most closely related (98 to 100% identity) to sequences detected in various subseafloor benthic sedimentary habitats including gas-hydrate-bearing sediments and in other near-surface habitats associated with hydrocarbon seepage (*SI Appendix*, Fig. S6). Close relatives of two gas-associated *Sulfurovum* ASVs were detected only in near-seafloor oxic habitats such as cold seeps and hydrothermal vent fluids (*SI Appendix*, Fig. S6). This agrees with *Sulfurovum* not being detected in the deeper core sections in our study (Fig. 4 *C* and *D*) and previous reports of *Sulfurovum* and other *Campylobacterota* inhabiting geofluid-impacted surface sediments (33) and not deeper sediment layers.

Metagenome-Assembled Genomes of Gas-Associated Lineages. Shotgun metagenome sequencing from three sediments including a gas-positive location followed by coassembly and binning resulted in the reconstruction of 14 metagenome-assembled genomes (MAGs) affiliated with the four gas-associated lineages (*Atribacteria* = 5, *Aminicenantes* = 5, *Sulfurovum* = 1, and *Thermoprofundales* = 3; *SI Appendix*, Table S4). Together these 14 MAGs corresponded to >25% of the total reads in the gas-positive sediment metagenome (Fig. 6), consistent with the amplicon sequencing results indicating high abundance of these organisms (Fig. 4*A*). Respiratory genes including cytochrome *c* oxidase, periplasmic nitrate reductase, sulfur oxidation, and sulfide-quinone reductase were only detected in the *Sulfurovum* MAG, not in the MAGs of the three other lineages. The *Sulfurovum* MAG also contained a complete reductive tricarboxylic acid (rTCA) cycle for autotrophic carbon fixation, consistent with the presence of this pathway in all previously described autotrophic members of *Campylobacterota* (22). This suggests a respiratory lithoautotrophic lifestyle fueled by inorganic sulfur compounds. In contrast to *Sulfurovum*, the 13 MAGs affiliated with *Atribacteria*, *Aminicenantes*, and *Thermoprofundales* showed evidence for fermentative degradation of organic matter. Acetogenesis has been postulated as an important process for energy metabolism in the deep subsurface (34). In agreement with this, potential for acetogenesis was observed in all three lineages with three out of the five *Aminicenantes* MAGs containing genes for the Wood–Ljungdahl pathway (Fig. 6). A variety of predicted extracellular and intracellular peptidases were observed in MAGs from all three lineages. In particular, MAGs encoding extracellular peptidases gingipain (Merops family C25) and clostripain (Merops family C11) were encoded by *Thermoprofundales* and *Atribacteria*, respectively. These extracellular enzyme families have been implicated in detrital protein degradation in the subseafloor by these lineages (27, 28). Hydrogen metabolism genes were also detected with *Aminicenantes*, *Thermoprofundales*, and *Atribacteria* MAGs encoding putative cytosolic group 3 [NiFe]-hydrogenases (Fig. 6). These enzymes couple NAD(P)H reoxidation to fermentative hydrogen production (35). *Atribacteria* MAGs also encoded putative groups 1 and 4 [NiFe]-hydrogenases consistent with fermentative hydrogen production and previous reports that these bacteria are anaerobic heterotrophs (36). Genes for acetogenesis, hydrogen production, and peptide degradation are indicative of fermentative lifestyles found in microbes inhabiting deep subseafloor sediments.

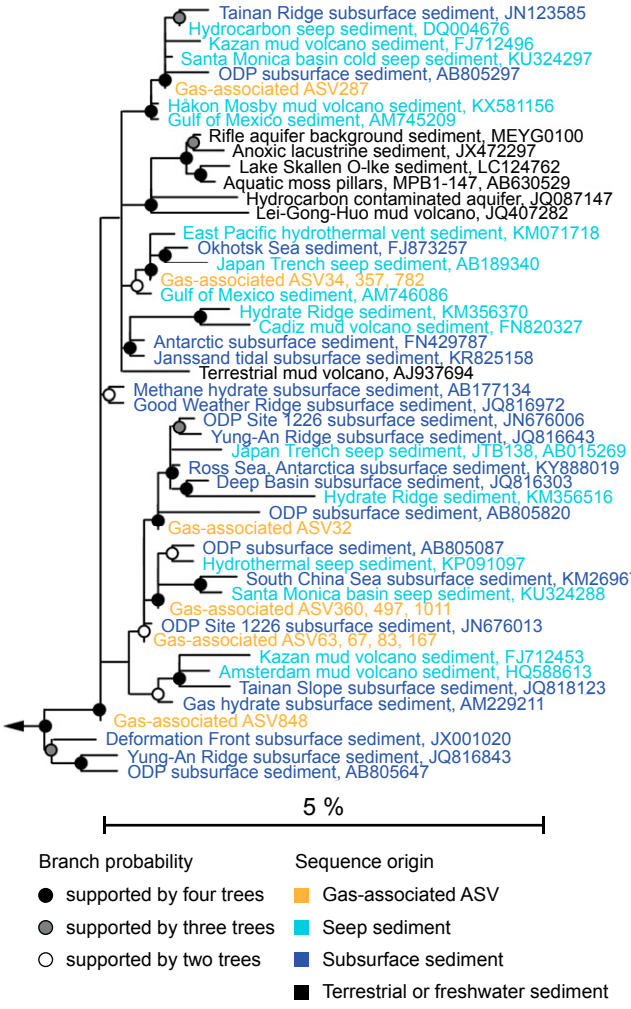

Fig. 5. Phylogeny of *Atribacteria* based on full-length 16S rRNA gene sequences from diverse environments. Gas-associated ASVs along with their closest relatives (minimum sequence identity for inclusion 98%) are shown. This consensus tree is based on four separate phylogenetic reconstructions (phyML, RAxML, RAxML8, and neighbor-joining), with shaded nodes indicating the number of individual trees that gave rise to the same branching pattern, i.e., black nodes signify microbial lineages that are very stable independent of the phylogenetic algorithm, and that have high bootstrap support (typically >95%; not shown). An extended tree (*SI Appendix*, Fig. S5) showing the phylogeny of all *Atribacteria* ASVs detected in this study is included in *SI Appendix*.

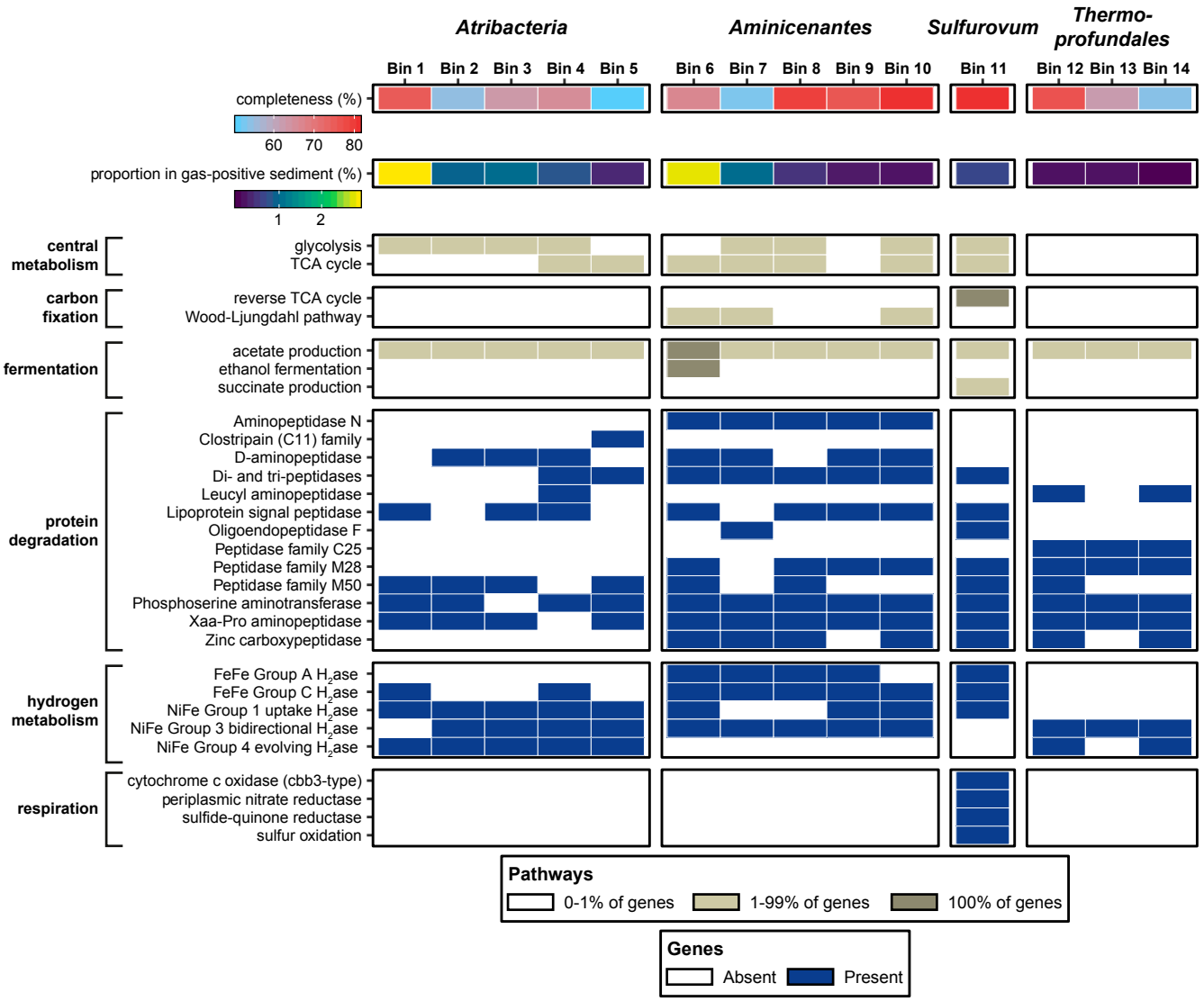

Fig. 6. Metagenome-assembled genomes affiliated with the gas-associated bacteria and archaea. Fourteen MAGs were affiliated with the four gas-associated lineages. Heat maps show genome completeness, relative abundance in a gas-positive sediment (based on mapping against total unassembled reads), and the relative proportions of different metabolic pathways involved in central metabolism, carbon fixation, and protein degradation detected in each MAG. The presence or absence of additional genes of interest related to protein degradation, hydrogen metabolism, and respiration, are also indicated.

Discussion

Sedimentary deposits within the Gulf of Mexico basin are characterized by enormous amounts of natural oil and gas seepage, sourced from the underlying petroleum-bearing reservoirs (6). Hydrocarbon movement through porous sediment layers is typically controlled by a multitude of factors including fluid buoyancy, fracture stability, sediment morphology, and pore pressure in the sediment column (21). Migrating geofluids are highly variable in their composition, often containing deeply sourced thermogenic oil and gas mixed with biogenic methane produced in the overlying anoxic sedimentary layers (10). This effect was observed in the 11 gas-positive sediments studied here, which all contained >10,000 ppmv of light alkane gases. Plotting the gas data from these sediments together with historic data from sediments sampled similarly in the Central and Western GoM basin shows that these characteristics are representative of >200 additional locations (*SI Appendix*, Fig. S1) demonstrating that vigorous gas seepage is widespread in the Gulf of Mexico.

The presence of gaseous hydrocarbons greatly contributes to the overall buoyant force of the migrating fluids which in turn is crucial for maintaining a steady, pressure-driven upward flow through the sediment layers (37). Only 11 cores showed evidence of this continuous advection of gas and oil, which is a small fraction compared to the large majority of the cores ($n = 121$) containing only thermogenic oil, suggesting weak, discontinuous or even permanently ceased geofluid seepage in most locations. Detecting thermogenic C_{2+} gases in all 11 gas-positive locations (Fig. 2*A*) further indicates that gas-derived buoyancy was present at deeply buried petroleum accumulations where fluid migration would have initiated. Entrainment of biogenic gases, whether from the same deep layers or from overlying methanogenic sediments likely increases the buoyancy and therefore the advective capacity of the geofluid flow.

Microbial community comparisons revealed that near-seafloor sediments in the 11 gas-positive locations harbored a distinct microbiome (Fig. 3). By contrast, the presence of migrated oil did not significantly affect surface sediment microbial community composition. Hydrocarbons advecting up from the subsurface together with distinct microbial communities in the near-surface sediments point toward the development of a microbial

ecosystem in these gas seeps influenced not only by energy-rich geofluids but also by immigrating microbes traveling up from the subsurface together with the fluids. Other indications of subsurface-to-seafloor dispersal include recent observations of a lineage of *Atribacteria* in surficial sediment at an active marine mud volcano on the Norwegian continental slope (15), and another lineage of *Atribacteria* in the bottom water overlying a mud volcano offshore Japan (14). In the present study, anomalies of multiple subsurface lineages of not only *Atribacteria* but also *Aminicenantes* and archaeal *Thermoprofundales* (Fig. 4) across multiple cold seeps demonstrate this phenomenon to be much more widespread. Associations of subsurface microbial groups with gaseous thermogenic hydrocarbons suggest deep-to-shallow dispersal of diverse populations at cold seeps is a persistent feature in the deep sea.

The deep biosphere provenance of these lineages is supported by various community surveys (14, 25, 26, 28, 32). The majority of the gas-associated ASVs identified in our study belonged to *Atribacteria* that cluster within distinct clades of sequences almost exclusively derived from subseafloor habitats and hydrocarbon seeps (Fig. 5). The updated high-resolution phylogeny reported here reveals *Atribacteria* to be a relatively narrow clade, with closely related members likely representing very similar metabolic and ecological niches (*SI Appendix*, Fig. S5). It also suggests that *Atribacteria* evolve slowly, possibly due to very long generation times in the subsurface (38), where fewer stressors may also contribute to lower rates of evolution (39). *Atribacteria* also seem to be sensitive to oxygen as their populations have been shown to disappear upon exposure to the oxygenated seafloor at a mud volcano (15), and increase in relative abundance in anoxic layers of coastal sediment (32). Seabed oxygen penetration at cold seeps tends to be very shallow, e.g., <1 to 2 cmbsf (40), thereby establishing anoxic, reduced conditions similar to deeper subsurface environments in near-surface sediment layers (12). Due to the large depth interval (20 cm) of the core sections in our study, we were unable to determine whether or not *Atribacteria* were present precisely in oxic surficial sediment layers. Indeed, differentiating between migrant cells arriving via upward dispersal, and their descendants that may have proliferated in situ, requires deeper cores sampled at higher resolution. Geofluid-supplied cells from below together with maintenance of anoxic subsurface-like conditions near to the surface by geofluid migration likely allow migrant *Atribacteria* to survive and proliferate in the gas-positive locations. Relative abundances of up to 2% for gas-associated ASVs in these sediments support this interpretation (*SI Appendix*, Fig. S4).

It is likely that different *Atribacteria* share a relatively large proportion of genes and pathways such that the present number of metagenome-assembled and single-cell genomes from the classes OP9 and JS1 (28, 36, 41) may provide a comprehensive picture of the ecological niches realized by members of this phylum. Currently available *Atribacteria* genomes provide evidence that these organisms are capable of fermentative degradation of organic matter (36, 42). The metabolic potential inferred from *Atribacteria* MAGs in this study is consistent with those findings, showing no evidence for aerobic metabolism (Fig. 6). Similar metabolic capabilities have been proposed for the archaeal *Thermoprofundales* that are widespread in the marine subsurface (23). Single-cell genomic sequencing of a *Thermoprofundales* from the subsurface showed potential for extracellular protein degradation using enzymes that are abundant in anoxic deep marine sediments (27). The same families of extracellular proteases were detected in all *Thermoprofundales* MAGs retrieved here (Fig. 6). A lifestyle based on degradation of detrital amino acids in subsurface sediments has also been proposed for *Aminicenantes* (28) highlighted here as a deep biosphere clade that can be detected in cold seep sediments. Genomics for these lineages points to an anaerobic heterotrophic lifestyle which is consistent with the prominence of these taxa in anoxic deep sediments (28, 43), and in contrast to the metabolic requirements for living at the sediment–water interface.

Two ASVs within the genus *Sulfurovum* also showed strong correlation with the gas parameters (Fig. 4*E* and *SI Appendix*, Table S3). Unlike the three subsurface-derived lineages discussed above, *Sulfurovum* was not detected in the deeper core sections (Fig. 4 *C* and *D*). Members of this genus are well known for their aerobic chemolithoautotrophic lifestyle in oxic sediment layers where they oxidize high-energy electron donors. As expected, the *Sulfurovum* MAG in our study contains respiratory genes along with a complete carbon fixation pathway (Fig. 6). The phylogeny of *Sulfurovum* ASVs and their close relatives (*SI Appendix*, Fig. S6) confirms that they are not found in deeply buried sediments but rather colonize hydrothermal vents and sulfidic near-surface sediment horizons of hydrocarbon seeps (33). In EGoM sediments, *Sulfurovum* may be present at higher abundances at the sediment–water interface than the levels revealed in these sequencing libraries, which represent an aggregate signal for 0 to 20 cmbsf. Quantitative assays specific for different lineages would need to be applied at finer depth resolution to reveal spatial variance in population densities of seep-colonizing and subsurface-derived groups in settings like these. Similar relative abundances at the surface for most gas-associated *Atribacteria*, *Aminicenantes*, *Thermoprofundales*, and *Sulfurovum* ASVs (*SI Appendix*, Fig. S4) suggest that all of these groups may exhibit activity in the shallow sediment layers in situ, although not necessarily at the same precise depths.

Coexistence of subseafloor lineages in near-surface EGoM sediments, their association with hydrocarbon gas emission, their elevated abundance at greater sediment depth, and their physiological potential revealed by genomics suggest that *Atribacteria*, *Aminicenantes*, and *Thermoprofundales* are dispersed from deeper sediment layers by the upward migration of hydrocarbons. Continuous emission of geofluids could alter the sediment habitat near the sediment–water interface and maintain subsurface-like conditions that allow migrant *Atribacteria*, *Aminicenantes*, and *Thermoprofundales* to survive. Previous work in the same study area presented evidence that thermophilic spores passively migrate up to the surface from underlying warm petroleum-bearing sediments via hydrocarbon seepage (13). Whereas dormant endospores remain unaffected by selection pressure from the near-surface conditions and could be correlated to the presence of oil regardless of the continuity of active buoyant seepage, the gas-associated *Atribacteria*, *Aminicenantes*, and *Thermoprofundales* identified in this study likely play a metabolic role in seep ecosystems owing to their consistently high relative abundance in cold seep surface sediments where conditions may more closely resemble the subsurface. This points to hydrocarbon seepage as an important dispersal vector and determinant of microbial biogeography and diversity in the Gulf of Mexico, where gas seepage is widespread (*SI Appendix*, Fig. S1*B*). Redistribution of subsurface microbes into the deep sea enables their deposition in near-surface environments where they may contribute to local biogeochemical cycling where conditions permit, before reentering the deep biosphere via sedimentation over longer timescales.

Methods

Sampling of Marine Sediments. Marine sediments were collected during January–March 2011, aboard RV GeoExplorer as part of TDI-Brooks International's Surface Geochemical Exploration (SGE) program. Piston cores penetrating 2.2 to 5.8 m below seafloor (mbsf) were collected and immediately extruded into 20-cm sections. Sediments for microbiological analyses were collected from the uppermost section, i.e., 0 to 20 cmbsf for all locations, whereas additional samples were collected from two deeper sections (40 to 60 and 80 to 100 cmbsf) from four locations. Sediment samples were sealed in sterile Whirl-Pak bags with minimal air exposure and kept frozen at −20 °C. Sediment sections from the bottom half of each piston core were

also frozen at −20 °C for hydrocarbon analysis (44). Portions of these bottom sections were placed in 500-mL gas canisters containing 160 mL clean, degassed, and sterilized seawater for analysis of interstitial light hydrocarbon gases. Canisters were sealed immediately after flushing the headspace with purified nitrogen and stored at −20 °C.

Hydrocarbon Characterization. Concentrations of interstitial light hydrocarbon gases were measured from the sediment samples stored in gas canisters. Frozen sediments in canisters were allowed to thaw and a silicone septum was silicone glued to each lid, followed by canisters being placed at 40 °C for at least 4 h. Light hydrocarbons dissolved in the interstitial water were subsequently equilibrated with the nitrogen gas phase by vigorous agitation for 5 min using a high-speed shaker. Hydrocarbon gases in these equilibrated samples were measured using gas chromatography coupled with flame ionization detection. Responses for each analyte were compared to a calibration curve (constructed using an external standard mixture of five hydrocarbon gases) to derive the concentration of each gas partitioned into the canister's headspace. Concentrations (in ppmv) of each gas originally in the sediment were calculated from the volumes of sediment and headspace in the canister and equilibrium partition coefficients for each compound. Gas isotopic composition was determined using gas chromatography combustion isotope ratio mass spectrometry (GC-C-IRMS; see *SI Appendix* for details). Liquid hydrocarbon analysis was performed on solvent extracts prepared from three equidistant segments within the bottom half of each piston core (see *SI Appendix, Supplementary Methods* for additional details). Frozen sediments were thawed, oven dried, and 15-g portions were solvent extracted with hexane using an automated extraction apparatus (Dionex ASE200). Oil parameters (UCM and TSF intensities) were subsequently measured from these extracts.

16S rRNA Gene Amplicon Sequencing. Genomic DNA was extracted from 0.5 to 1.0 g of sediment from each sample using the DNeasy PowerLyzer PowerSoil Kit (12855-100, QIAGEN) according to manufacturer protocol with minor modifications for the step of homogenization and cell lysis, i.e., cells were lysed by bead beating at 6 m s^{-1} for 45 s using a Bead Ruptor 24 (OMNI). Extraction blanks were performed alongside the samples to assess laboratory contamination during the extraction process. DNA concentrations were assessed fluorometrically using a Qubit 2.0 fluorometer (Thermo Fisher Scientific). The v3-4 region of the bacterial 16S rRNA gene and the v4-5 region of the archaeal 16S rRNA gene were amplified using the primer pairs SD-Bact-0341-bS17/SD-Bact-0785-aA21 and SD-Arch-0519-aS15/SD-Arch-0911-aA20, respectively (45), followed by post-PCR cleanup and indexing. Indexed amplicon samples were sequenced using Illumina's v3 600-cycle (paired-end) reagent kit on an Illumina MiSeq benchtop sequencer (Illumina Inc.) after all DNA extraction blanks and PCR reagent blanks were confirmed for negative amplification. Raw sequences were quality controlled and further processed to construct an ASV table. Detailed methods for PCR conditions, amplicon cleanup, indexing, sequence processing, ASV taxonomy assignment, estimation of alpha and beta diversity, and associated statistical analyses are described in *SI Appendix*.

Phylogenetic Analyses. Phylogenetic analyses were conducted based on 16S rRNA gene sequences from the SILVA database SSU Ref NR 132 (29). For an up-to-date phylogeny of *Atribacteria*, the NCBI database (as of June 2018) was searched against selected *Atribacteria* full-length sequences using blastn with a match/mismatch score of 1/−1 to allow for broad hits. The nonredundant SILVA reference tree was subsequently updated by adding sequences retrieved from NCBI. From the resulting 1,757 nonredundant sequences affiliated with *Atribacteria*, those that were nearly full length (>1,350 nucleotides) and had an alignment quality score of >94 were retained, resulting in 698 sequences. After retaining sequences from diverse ecosystems, while removing close relatives from the same ecosystem, the remaining 217 sequences were aligned using SINA (46). The alignment was then manually curated based on ribosomal secondary structure and subsequently used to calculate trees using four different algorithms (phyML, RAxML, RAxML8, and neighbor-joining). For each tree we used the same positional variability filter including only conserved positions in the alignment with a mutation rate of less than 3.1%. The final alignment included 1,126 valid columns encompassing *Escherichia coli* reference positions 1,784 to 42,529. Each tree was calculated with 100 iterations after which the most robust tree was selected. Four resulting trees were used to calculate a consensus tree using the tool as implemented in ARB (47). Finally, the short ASV sequences from this study were added to the consensus tree using the same positional variability filter without changing the overall tree topology. Phylogeny construction of the other groups is described in *SI Appendix*.

Metagenome Library Preparation, Sequencing, and Analyses. For metagenome library preparation, DNA was extracted from ∼10 g of sediment from three different locations using the PowerMax Soil Kit (12988-10, QIAGEN) according to the manufacturer's protocol. Cells were lysed by bead beating for 45 s at 5.5 m s^{-1}, followed by fluorometric assessment of DNA concentrations. Metagenomic library preparation and DNA sequencing was conducted at the Center for Health Genomics and Informatics in the Cumming School of Medicine, University of Calgary. Genomic DNA was sheared using a Covaris sonicator, and DNA fragment libraries were subsequently prepared using a NEBNext Ultra II DNA Library Prep Kit for Illumina (New England BioLabs). Metagenomic libraries were sequenced using a ∼40 Gb (i.e., 130 M reads) midoutput 300 cycle (2 × 150 bp) sequencing kit on an Illumina NextSeq 500 System. Detailed methods of raw read processing, assembly, mapping, binning, and annotation are provided in *SI Appendix*.

ACKNOWLEDGMENTS. We wish to thank Jody Sandel as well as the crew of R/V GeoExplorer for collection of piston cores, onboard core processing, sample preservation, and shipment. Cynthia Kwan and Oliver Horanszky are thanked for assistance with amplicon library preparation. We also wish to thank Jayne Rattray, Daniel Gittins, and Marc Strous for valuable discussions and suggestions, and Rhonda Clark for research support. Collaborations with Andy Mort from the Geological Survey of Canada, and Richard Hatton from Geoscience Wales are also gratefully acknowledged. This work was financially supported by a Mitacs Elevate Postdoctoral Fellowship awarded to A.C.; an Alberta Innovates-Technology Futures/Eyes High Postdoctoral Fellowship to S.E.R.; and a Natural Sciences and Engineering Research Council Strategic Project Grant, a Genome Canada Genomics Applications Partnership Program grant, a Canada Foundation for Innovation grant (CFI-JELF 33752) for instrumentation, and Campus Alberta Innovates Program Chair funding to C.R.J.H.

1. W. D. Orsi, Ecology and evolution of seafloor and subseafloor microbial communities. *Nat. Rev. Microbiol.* **16**, 671–683 (2018).
2. O. Plümper *et al*., Subduction zone forearc serpentinites as incubators for deep microbial life. *Proc. Natl. Acad. Sci. U.S.A.* **114**, 4324–4329 (2017).
3. F. Inagaki *et al*., DEEP BIOSPHERE. Exploring deep microbial life in coal-bearing sediment down to ∼2.5 km below the ocean floor. *Science* **349**, 420–424 (2015).
4. M.-C. Ciobanu *et al*., Microorganisms persist at record depths in the subseafloor of the Canterbury Basin. *ISME J.* **8**, 1370–1380 (2014).
5. B. N. Orcutt, J. B. Sylvan, N. J. Knab, K. J. Edwards, Microbial ecology of the dark ocean above, at, and below the seafloor. *Microbiol. Mol. Biol. Rev.* **75**, 361–422 (2011).
6. E. E. Cordes, D. C. Bergquist, C. R. Fisher, Macro-ecology of Gulf of Mexico cold seeps. *Annu. Rev. Mar. Sci.* **1**, 143–168 (2009).
7. E. Suess, "Marine cold seeps: Background and recent advances" in *Hydrocarbons, Oils and Lipids: Diversity, Origin, Chemistry and Fate*, H. Wilkes, Ed. (Springer International Publishing, Cham, 2018), pp. 1–21.
8. A. J. Kopf, (2002) Significance of mud volcanism. *Rev. Geophys.* **40**, 2-1-2-52.
9. M. O. Schrenk, J. A. Huber, K. J. Edwards, Microbial provinces in the subseafloor. *Annu. Rev. Mar. Sci.* **2**, 279–304 (2010).
10. C. Hubert, A. Judd, (2010) "Using microorganisms as prospecting agents in oil and gas exploration" in *Handbook of Hydrocarbon and Lipid Microbiology*, K. N. Timmis Ed. (Springer Berlin Heidelberg, Berlin, Heidelberg), pp. 2711–2725.
11. D. H. Case *et al*., Methane seep carbonates host distinct, diverse, and dynamic microbial assemblages. *MBio* **6**, e01348-15 (2015).
12. S. E. Ruff *et al*., Global dispersion and local diversification of the methane seep microbiome. *Proc. Natl. Acad. Sci. U.S.A.* **112**, 4015–4020 (2015).
13. A. Chakraborty *et al*., Thermophilic endospores associated with migrated thermogenic hydrocarbons in deep Gulf of Mexico marine sediments. *ISME J.* **12**, 1895–1906 (2018).
14. T. Hoshino *et al*., Atribacteria from the subseafloor sedimentary biosphere disperse to the hydrosphere through submarine mud volcanoes. *Front. Microbiol.* **8**, 1135 (2017).
15. S. E. Ruff *et al*., In situ development of a methanotrophic microbiome in deep-sea sediments. *ISME J.* **13**, 197–213 (2019).
16. A. G. Judd, The global importance and context of methane escape from the seabed. *Geo-Mar. Lett.* **23**, 147–154 (2003).
17. S. S. S. Cardoso, J. H. E. Cartwright, Increased methane emissions from deep osmotic and buoyant convection beneath submarine seeps as climate warms. *Nat. Commun.* **7**, 13266 (2016).
18. A. Vigneron *et al*., Comparative metagenomics of hydrocarbon and methane seeps of the Gulf of Mexico. *Sci. Rep.* **7**, 16015 (2017).
19. S. Kleindienst *et al*., Diverse sulfate-reducing bacteria of the *Desulfosarcina/Desulfococcus* clade are the key alkane degraders at marine seeps. *ISME J.* **8**, 2029–2044 (2014).
20. D. T. Wang *et al*., Methane cycling. Nonequilibrium clumped isotope signals in microbial methane. *Science* **348**, 428–431 (2015).
21. M. A. Abrams, Significance of hydrocarbon seepage relative to petroleum generation and entrapment. *Mar. Pet. Geol.* **22**, 457–477 (2005).

22. A. Assié *et al*., Horizontal acquisition of a patchwork Calvin cycle by symbiotic and free-living Campylobacterota (formerly Epsilonproteobacteria). *ISME J.* **14**, 104–122 (2020).
23. Z. Zhou *et al*., Genomic and transcriptomic insights into the ecology and metabolism of benthic archaeal cosmopolitan, Thermoprofundales (MBG-D archaea). *ISME J.* **13**, 885–901 (2019).
24. M. I. Love, W. Huber, S. Anders, Moderated estimation of fold change and dispersion for RNA-seq data with DESeq2. *Genome Biol.* **15**, 550 (2014).
25. F. Inagaki *et al*., Biogeographical distribution and diversity of microbes in methane hydrate-bearing deep marine sediments on the Pacific Ocean Margin. *Proc. Natl. Acad. Sci. U.S.A.* **103**, 2815–2820 (2006).
26. S. A. Carr, B. N. Orcutt, K. W. Mandernack, J. R. Spear, Abundant Atribacteria in deep marine sediment from the Adélie Basin, Antarctica. *Front. Microbiol.* **6**, 872 (2015).
27. K. G. Lloyd *et al*., Predominant archaea in marine sediments degrade detrital proteins. *Nature* **496**, 215–218 (2013).
28. J. T. Bird *et al*., Uncultured microbial Phyla suggest mechanisms for multi-thousand-year subsistence in Baltic Sea sediments. *MBio* **10**, e02376-18 (2019).
29. C. Quast *et al*., The SILVA ribosomal RNA gene database project: Improved data processing and web-based tools. *Nucleic Acids Res.* **41**, D590–D596 (2013).
30. P. Yarza *et al*., Uniting the classification of cultured and uncultured bacteria and archaea using 16S rRNA gene sequences. *Nat. Rev. Microbiol.* **12**, 635–645 (2014).
31. J. B. Glass *et al*., Adaptations of *Atribacteria* to life in methane hydrates: Hot traits for cold life. *bioRxiv*, 10.1101/536078 (31 January 2019).
32. C. Petro *et al*., Marine deep biosphere microbial communities assemble in near-surface sediments in Aarhus Bay. *Front. Microbiol.* **10**, 758 (2019).
33. N. H. Akerman, D. A. Butterfield, J. A. Huber, Phylogenetic diversity and functional gene patterns of sulfur-oxidizing subseafloor Epsilonproteobacteria in diffuse hydrothermal vent fluids. *Front. Microbiol.* **4**, 185 (2013).
34. M. A. Lever, Acetogenesis in the energy-starved deep biosphere–A paradox? *Front. Microbiol.* **2**, 284 (2012).
35. X. Dong *et al*., Metabolic potential of uncultured bacteria and archaea associated with petroleum seepage in deep-sea sediments. *Nat. Commun.* **10**, 1816 (2019).
36. M. K. Nobu *et al*., Phylogeny and physiology of candidate phylum 'Atribacteria' (OP9/JS1) inferred from cultivation-independent genomics. *ISME J.* **10**, 273–286 (2016).
37. A. M. Abrams, Evaluation of near-surface gases in marine sediments to assess subsurface petroleum gas generation and entrapment. *Geosciences* **7**, 35 (2017).
38. B. B. Jørgensen, I. P. G. Marshall, Slow microbial life in the seabed. *Annu. Rev. Mar. Sci.* **8**, 311–332 (2016).
39. S.-J. Li *et al*., Microbial communities evolve faster in extreme environments. *Sci. Rep.* **4**, 6205 (2014).
40. P. Pop Ristova, F. Wenzhöfer, A. Ramette, J. Felden, A. Boetius, Spatial scales of bacterial community diversity at cold seeps (Eastern Mediterranean Sea). *ISME J.* **9**, 1306–1318 (2015).
41. J. A. Dodsworth *et al*., Single-cell and metagenomic analyses indicate a fermentative and saccharolytic lifestyle for members of the OP9 lineage. *Nat. Commun.* **4**, 1854 (2013).
42. Y. M. Lee *et al*., Genomic insight into the predominance of candidate Phylum Atribacteria JS1 lineage in marine sediments. *Front. Microbiol.* **9**, 2909 (2018).
43. C. Pelikan *et al*., Glacial runoff promotes deep burial of sulfur cycling-associated microorganisms in marine sediments. *Front. Microbiol.* **10**, 2558 (2019).
44. M. A. Abrams, F. D. Nicola, Surface sediment hydrocarbons as indicators of subsurface hydrocarbons: Field calibration of existing and new surface geochemistry methods in the Marco Polo area, Gulf of MexicoSurface sediment hydrocarbons as indicators of subsurface hydrocarbons. *AAPG Bull.* **95**, 1907–1935 (2011).
45. A. Klindworth *et al*., Evaluation of general 16S ribosomal RNA gene PCR primers for classical and next-generation sequencing-based diversity studies. *Nucleic Acids Res.* **41**, e1 (2013).
46. E. Pruesse, J. Peplies, F. O. Glöckner, SINA: Accurate high-throughput multiple sequence alignment of ribosomal RNA genes. *Bioinformatics* **28**, 1823–1829 (2012).
47. W. Ludwig *et al*., ARB: A software environment for sequence data. *Nucleic Acids Res.* **32**, 1363–1371 (2004).